









# Echoes from Beyond: Detecting Gravitational Wave Quantum Imprints with LISA

Nils Deppe <sup>1,2,3</sup> Lavinia Heisenberg<sup>4</sup> Henri Inchauspé <sup>5,6</sup> Lawrence E. Kidder <sup>3</sup> David Maibach <sup>4,\*</sup> Sizheng Ma,<sup>7</sup> Jordan Moxon <sup>8</sup> Kyle C. Nelli <sup>8</sup> William Throwe <sup>3</sup> and Nils L. Vu <sup>8</sup>

<sup>1</sup>Laboratory for Elementary Particle Physics, Cornell University, Ithaca, New York 14853, USA

<sup>2</sup>Department of Physics, Cornell University, Ithaca, NY, 14853, USA

<sup>3</sup>Cornell Center for Astrophysics and Planetary Science, Cornell University, Ithaca, New York 14853, USA

<sup>4</sup>Institute for Theoretical Physics, University of Heidelberg,  
Philosophenweg 16 D-69120 Heidelberg, Germany

<sup>5</sup>Institute for Theoretical Physics, KU Leuven, Celestijnenlaan 200D, B-3001 Leuven, Belgium

<sup>6</sup>Leuven Gravity Institute, KU Leuven, Celestijnenlaan 200D box 2415, 3001 Leuven, Belgium

<sup>7</sup>Perimeter Institute for Theoretical Physics, Waterloo, ON N2L2Y5, Canada

<sup>8</sup>Theoretical Astrophysics 350-17, California Institute of Technology, Pasadena, CA 91125, USA  
(Dated: November 11, 2024)

We assess the prospects for detecting gravitational wave echoes arising due to the quantum nature of black hole horizons with LISA. In a recent proposal, Bekenstein’s black hole area quantization is connected to a discrete absorption spectrum for black holes in the context of gravitational radiation. Consequently, for incoming radiation at the black hole horizon, not all frequencies are absorbed, raising the possibility that the unabsorbed radiation is reflected, producing an echo-like signal closely following the binary coalescence waveform. In this work, we further develop this proposal by introducing a robust, phenomenologically motivated model for black hole reflectivity. Using this model, we calculate the resulting echoes for an ensemble of Numerical Relativity waveforms and examine their detectability with the LISA space-based interferometer. Our analysis demonstrates promising detection prospects and shows that, upon detection, LISA provides a direct probe of the Bekenstein-Hawking entropy. In addition, we find that the information extractable from LISA data offers valuable constraints on a wide range of quantum gravity theories.

PACS numbers: 98.80.Cq

**Introduction.** Classically, the black hole (BH) horizon is considered an unremarkable region of spacetime, with no distinctive effects expected locally. However, in the quantum regime, this picture may change dramatically, as indicated initially by Hawking’s predictions of thermal radiation being emitted by a BH [1]. Although the precise quantum structure of a BH’s horizon remains unknown, numerous theories have been proposed to model its quantum properties. These include the membrane paradigm [2–4] (see also [5, 6]), effective field theories [7] and phenomenological approaches [8]. Another straightforward ansatz based on the Bekenstein-Mukhanov model of BH quantization has been recently proposed in [9]: Using a Bohr-Sommerfeld-like quantization framework and first principles, Bekenstein and Mukhanov argued that BHs develop a discrete area spectrum, given by  $A_N = \alpha \ell_{\text{Pl}}^2 N$ , where  $\ell_{\text{Pl}}$  is the Planck length and  $N$  a positive integer. The phenomenological constant  $\alpha$  is determined by the underlying theory of quantum gravity (in semi-classical computations, it is set to be  $8\pi$ ). The area quantization directly implies a discrete mass spectrum, leading to the quantization of BH emission and absorption processes. Concretely, only frequencies within the spectrum

$$\omega = \frac{|\Delta M|}{\hbar} = \frac{\alpha \Delta N}{32\pi M}, \quad (1)$$

can be absorbed or emitted, where  $M$  is the mass of the BH and  $\Delta N$  the number of microstates. As these frequencies scale in  $1/M$ , Planck-scale effects are magnified, pushing them into the realm of detectability for gravitational wave (GW) interferometers [9]. Taking into account the spin of the BH and the fact that, in astrophysical context, we encounter only macroscopic BHs, i.e.,  $N \gg 1$ , one can compute the characteristic frequencies of the BH as a function of the phenomenological constant,  $\alpha$ , and dimensionless spin,  $a$ , as [9]

$$\omega_N(\alpha) = \frac{\kappa \alpha N}{8\pi} + 2\Omega_H + \mathcal{O}(N^{-1}), \quad (2)$$

where  $\kappa = \frac{\sqrt{1-a^2}}{2M(1+\sqrt{1-a^2})}$  and  $\Omega_H = \frac{a}{2M(1+\sqrt{1-a^2})}$ . Here,  $\kappa$  and  $\Omega_H$  denote the surface gravity and the angular momentum, respectively.

The discrete spectrum implies that a significant portion of the GW ringdown modes may not be absorbed by a quantum black hole (QBH). As discussed in [10, 11], the unabsorbed modes could be reflected, resulting in a late-time echo in the gravitational waveform. A delayed GW echo reaching the detector is generally predicted by a manifold of phenomenology. This includes deviations from GR [12, 13], the presence of near-horizon (quantum) structure surrounding the BH [8, 10, 14–19] as well as the existence of exotic compact objects (ECOs) replacing the traditional BH by substituting the would-be horizon with a physical boundary [20–24]. In particular, in the context of near-horizon quantum structure, the

\* d.maibach@thphys.uni-heidelberg.de

echo manifests irrefutable evidence of an interplay between quantum physics and gravity [6, 8, 16]. As in [10], in this work, we focus on modifications due to quantumness appearing solely close to the horizon. The possibility of the BH quantum nature affecting, for instance, the effective potential of the BH, spanning all the way to the “photon sphere”, was already discussed in [11]. The potential detection of these echo signatures by current and future GW interferometers has been extensively studied in the literature, e.g., [25–27]. Note, however, that generally, the question of whether BHs or, alternatively, ECOs can produce echoes is still under debate, as highlighted in [28, 29] and [30, 31]. For ECOs, their stability is particularly critical for the generation of GW echoes [32, 33]. In this work, we do not aim to resolve this ongoing debate. Instead, we present a rigorous case study on the potential detection of echo-like signatures with the Laser Interferometer Space Antenna (LISA) [34], demonstrating that such echoes could serve as a smoking gun for advancing our understanding of BH physics.

Throughout this work, we adapt the assumptions that i) GR is our effective theory describing the dynamics of gravitational waves, ii) quantumness enters the GW solely via the discretization of absorbed and emitted frequencies, iii) the unabsorbed radiation is reflected off the BH. Naturally, iii) requires the definition of a reflectivity coefficient as well as a BH boundary condition for incoming radiation. In the following, we shall derive the latter step by step. We start by converting equation (1) and (2) into a robust reflectivity function, which will serve as the foundation for computing the resulting echo.

**Gravitational Waves from Quantum Black Holes: Reflectivity.** Modeling the reflectivity of QBH without additional information about the nature of the reflective surface requires careful consideration of various (quantum) effects. In this work, we adopt a simplified yet robust phenomenological model that captures a wide range of echo morphologies while remaining agnostic regarding the underlying theory of quantum gravity. Our approach is based on the assumption that the characteristic frequencies  $\omega_N$  appear as sharp lines in the QBH reflectivity spectrum resulting in an atom-like description for the BH, which is a direct consequence of the Bekenstein-Mukhanov proposal [35] (see also [10, 11] for further motivation). Treating the BH as an excited multilevel quantum system, spectral line broadening may occur. For the purposes of this work, it is particularly important to ensure that the BH’s energy levels do not overlap, as this would effectively cause the QBH to behave classically. As demonstrated by [9], the energy level’s thickness increase with the level of spin left in the remnant compact object. One finds, however, that for non-rotating BHs ( $a \ll 1$ ) the critical value for the phenomenological constant  $\omega_N(\alpha, a)$ , above which the spectrum exhibits no overlap, is much smaller than the smallest constant considered in literature, i.e.,  $\alpha = 4 \log 2$ . Nonetheless, the presence of quantum effects close to the horizon can turn the sharp roots of the reflectivity

into wider cusps around frequencies  $\omega_N$ . Examples of such quantum effects are discussed in the context of quantum modifications of the quasi-normal mode (QNM) spectrum [36, 37] and Hawking radiation [15, 38, 39].

Based on these assumptions, a first ansatz for the reflectivity reads

$$\mathcal{R}^{\text{QBH}} \sim \begin{cases} 1, & \omega \leq \omega_1, \\ \left| \sin \left( \frac{\pi \omega}{\omega_N(\alpha)} \right) \right|^\delta, & \omega > \omega_1, \end{cases} \quad (3)$$

where  $\delta$  parameterizes the “sharpness” of the spectral lines associated to  $\omega_N$ <sup>1</sup>. An equal spacing between the characteristic frequencies allows for the use of a periodic function. We will comment on exceptions to the assumption of equal spacing below.

On a quantum level, one has to acknowledge that the reflection of ingoing (towards the horizon) GWs is not the only emission channel for a BH. Already on a semi-classical level, Hawking radiation enters the arena, establishing an emission channel that is equally susceptible to the quantization arguments [40, 41]. In literature, the frequency corresponding to the Hawking temperature  $T_H$  commonly represents a bound beyond which the reflectivity is exponentially suppressed [6, 8, 16, 42, 43]. This assumption is frequently adapted in the realm of ECOs replacing BH and, in particular, is in concordance with the concept of BH microstates [44, 45]. Additional support for a suppression factor comes from astrophysical observations [46, 47] and discussions involving solutions to the BH information paradox [48, 49]. Thus, we adopt a conservative exponential suppression factor of  $\exp[-|\omega|/(2T_{QH})]$  in our ansatz for the reflectivity. Staying agnostic with respect to an alteration of the cut-off temperature, we replace the Hawking temperature with  $T_{QH} = \epsilon T_H$ , where the Hawking temperature is given by  $T_H = 1/8\pi$ . For  $T_{QH} \rightarrow 0$ , the reflectivity is fully suppressed and the classical limit is recovered.

So far, the reflectivity is purely real and does not contain information about potential phase shifts of the GWs upon reflection. To derive the latter, we now refine the setup leading to the production of echoes: We consider a cavity formed by the BH potential barrier and a shell surrounding the BH with a radius  $r_{\text{Shell}}$  slightly larger than the BH horizon. For ECOs, this shell resembles its (quantum) surface (or membrane). Here, we aim to stay as agnostic as possible regarding the shell’s properties, treating it as a fiducial surface (compare with discussions in [15]). By simple time delay arguments, the latter needs to be larger than the Schwarzschild radius  $r_H = 2M$  to find any detectable signal reaching an outside observer in finite time. As GWs reaching the horizon will not be observable, we thus choose  $r_{\text{Shell}} > r_H$ . Considering the Kerr horizons  $r_{\pm} = M(1 \pm \sqrt{1 - a^2})$ , where

<sup>1</sup>A nontrivial  $\delta$  effectively turns the absorption lines into cusps, a phenomena observed in many physical absorption spectra.

$a$  is the dimensionless spin parameter, the time a GW takes to complete a single cycle within the cavity is given by [42, 50]

$$\Delta t_{\text{echo}} = 2r^* \left| \frac{r_{\text{Barrier}}}{r_{\text{Shell}}} \right|, \quad (4)$$

where  $r^*$  is the tortoise coordinate. The latter implies [50]

$$\Delta t_{\text{echo}} \approx 2 \frac{r_+^2 + a^2 M^2}{r_+ - r_-} \ln \left( \frac{M}{r_{\text{Shell}} - r_+} \right) + M f(a), \quad (5)$$

where  $r_{\text{Shell}} - r_+ =: d_{\text{Shell}}^2 \sqrt{1 - a^2/4M(1 + \sqrt{1 - a^2})}$  and  $f(a) \approx 0.335/(a^2 - 1) + 4.77 + 7.42(a^2 - 1) + 4.69(a^2 - 1)^2$ . Equation (5) serves as a sufficient approximation to the exact formula, equation (4). The free parameter in this consideration is denoted as  $d_{\text{Shell}}$  and describes the proper distance between the fiducial shell,  $r_{\text{Shell}}$ , and the BH horizon,  $r_H$ . An intuitive sketch of the cavity is provided in Figure 1. In the limit of  $d_{\text{Shell}} \rightarrow 0$ , we obtain an infinite time separation between the echoes. Note however, that, in principle, the separation between echo and waveform can be arbitrary and information is lost by separating the initial waveform and its echo in the GW data (i.e., solely considering the strain corresponding to the echo). The existence of echoes with long time separation with respect to the sourcing waveform has been addressed in, e.g., [29].

Joining together the phase and amplitude modulation of the reflectivity implied by area quantization and setting  $a = 0$ , we obtain, using the convention  $M = 1$ ,

$$\mathcal{R}^{\text{QBH}} = e^{-i\omega 8 \ln(\beta)} e^{-\frac{|\omega|}{2T_{\text{QH}}}} \begin{cases} 1, & \omega \leq \omega_1, \\ \left| \sin \left( \frac{\pi\omega}{\omega_N(\alpha)} \right) \right|^\delta, & \omega > \omega_1, \end{cases} \quad (6)$$

where we have absorbed constant phase contributions through the introduction of a new model parameter  $\beta \sim d_{\text{Shell}}$ . Throughout this work, we set  $a = 0$  unless stated otherwise. This choice is primarily motivated by the desire to avoid the thickening of absorption lines and to simplify the computation of the echo as will be presented below. In principle, the reflectivity can easily be extended to spinning BHs by including the full expression in (2) and (5). In the limit  $\delta \rightarrow 0$  and with a suitable choice for  $\beta$ , one recovers the ECO reflectivity outlined in [8, 19]. In what follows, the reflectivity parameter  $\alpha, \beta, \epsilon$  and  $\delta$  define the parameter space for the echo model. With the model in (6), one can now construct the echo using the asymptotic gravitational radiation measured at the detector.

**Gravitational Waves from Quantum Black Holes: Echo.** In this work, the echo of a given GWs is computed following the methodology outlined in [51], where waveforms near the QBH are reconstructed using the asymptotic information encapsulated in the Newman

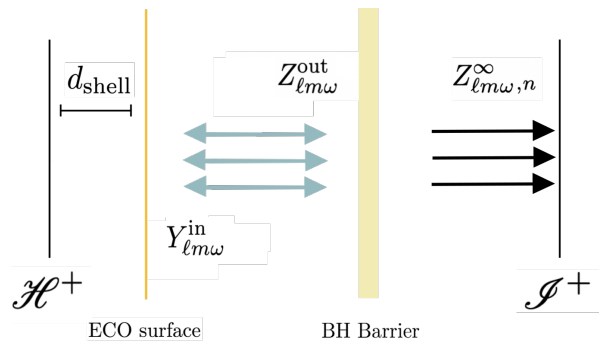


FIG. 1. Sketch of the cavity formed by the BH potential barrier and the reflective shell separated by  $d_{\text{Shell}}$  from the future BH horizon  $\mathcal{H}^+$ .

Penrose scalars  $\Psi_0^\circ$  and  $\Psi_4^\circ$  at future null infinity  $\mathcal{I}^{+2}$ . Physically, the generation of echoes during BH mergers proceeds as follows: After a binary system merges, the remnant BH is perturbed and undergoes a ringdown, emitting its QNM content. This process is described by the Teukolsky equation, which yields outgoing solutions towards  $\mathcal{I}^+$  and ingoing solutions towards the future QBH horizon  $\mathcal{H}^+$ . The ingoing waves become trapped in a cavity formed between the QBH’s fiducial reflective shell and the classical BH’s potential barrier. Since neither the potential barrier nor the reflective shell of the QBH is perfectly reflective, a portion of the gravitational radiation leaks out during each propagation cycle of radiation encapsulated by the cavity. This leads to an echo at  $\mathcal{I}^+$  and an energy flux across  $\mathcal{H}^+$ .

While the “initial” waveform can be computed via the asymptotic scalar  $\Psi_4^\circ$ , the subsequent echoes result from the ingoing radiation,  $\Psi_0^\circ$ . Both quantities can be computed at  $\mathcal{I}^+$  using numerical relativity codes. To connect this asymptotic information to the ingoing solution of the Teukolsky equation, the *hybrid approach* is utilized (see [51] and references therein). This approach reverse-engineers the ingoing radiation towards  $\mathcal{H}^+$  based on its asymptotic counterpart encapsulated in  $\Psi_0^\circ$ . Thereby, the corresponding GW is computed at the full spacetime boundary ( $\mathcal{I}^+ \cup \mathcal{I}^-$ ) imposing a no-ingoing boundary condition, the so-called *up-solution*. In this case, solving the Teukolsky equation, the asymptotic behavior of the radial coefficients of  $\Psi_4$  and  $\Psi_0$ , respectively, is described

<sup>2</sup>Technically,  $\Psi_4$  is not required to compute the echo, however, it provides information on the initial waveform reaching the detector without an echo.

by

$$-2R_{\ell m \omega} \sim \begin{cases} r^3 Z_{\ell m \omega}^{\infty} e^{i\omega r^*}, & r^* \rightarrow +\infty, \\ Z_{\ell m \omega}^{\text{out}} e^{i\omega r^*} + \Delta^2 Z_{\ell m \omega}^{\text{in}} e^{-i\omega r^*}, & r^* \rightarrow -\infty, \end{cases} \quad (7a)$$

$$+2R_{\ell m \omega} \sim \begin{cases} r^{-5} Y_{\ell m \omega}^{\infty} e^{i\omega r^*}, & r^* \rightarrow +\infty, \\ Y_{\ell m \omega}^{\text{out}} e^{i\omega r^*} + \Delta^{-2} Y_{\ell m \omega}^{\text{in}} e^{-i\omega r^*}, & r^* \rightarrow -\infty, \end{cases} \quad (7b)$$

where  $r^* \rightarrow -\infty$  describes the limit towards the future BH horizon,  $\mathcal{H}^+$ , and  $r^* \rightarrow \infty$  towards null infinity  $\mathcal{I}^+$ . The asymptotic information for  $\Psi_4^{\circ}$  ( $\Psi_0^{\circ}$ ) is encoded in  $Z_{\ell m \omega}^{\infty}$  ( $Y_{\ell m \omega}^{\infty}$ ) while  $Z_{\ell m \omega}^{\text{in}}$ ,  $Z_{\ell m \omega}^{\text{out}}$  ( $Y_{\ell m \omega}^{\text{in}}$ ,  $Y_{\ell m \omega}^{\text{out}}$ ) denote the amplitudes traveling towards and away from the horizon  $\mathcal{H}^+$  within the cavity described above, see Figure 1. The coefficients  $Z_{\ell m \omega}$ ,  $Y_{\ell m \omega}$  are related via the Teukolsky-Starobinsky (TS) relations [52, 53]

$$\begin{aligned} \frac{4\omega^4}{C} Y_{\ell m \omega}^{\infty} &= Z_{\ell m \omega}^{\infty}, \\ Y_{\ell m \omega}^{\text{in}} &= \frac{D}{C} Z_{\ell m \omega}^{\text{in}}, \end{aligned} \quad (8)$$

where

$$\begin{aligned} C &= (\ell - 1)\ell(\ell + 1)(\ell + 2) + 12i\omega, \\ D &= 64i\omega(128\omega^2 + 8)(1 - 2i\omega), \end{aligned} \quad (9)$$

and the reflectivity coefficients of the BH potential barrier, that are  $1/D_{\ell m \omega}^{\text{out}}$ ,  $D_{\ell m \omega}^{\text{in}}/D_{\ell m \omega}^{\text{out}}$  for outgoing and  $1/C_{\ell m \omega}^{\text{out}}$ ,  $C_{\ell m \omega}^{\text{in}}/C_{\ell m \omega}^{\text{out}}$  for ingoing radiation, see [51, 54, 55]. The latter are well-defined for multiple BH solutions (including the here considered case of linearly perturbed Schwarzschild BHs) and can be numerically determined using the Black-Hole Perturbation Toolkit [56].

Using the radial solutions (7) together with the reflectivity coefficients for QBH and the BH potential barrier, the radiation bouncing of the reflective shell,  $Z_{\ell m \omega}^{\text{out}}$ , can be computed using the ingoing contribution to  $\Psi_0$  in the limit  $r^* \rightarrow -\infty$ , i.e.,  $Y_{\ell m \omega}^{\text{in}}$  [51]. We stay agnostic with respect to the boundary conditions for the reflectivity of  $Y_{\ell m \omega}^{\text{in}}$  at the QBH's fiducial shell by assuming, inspired by [43],

$$Z_{\ell m \omega}^{\text{out QBH}} = \frac{(-1)^{\ell+m+1}}{\gamma} \mathcal{R}^{\text{QBH}} Y_{\ell m \omega}^{\text{in QBH}}, \quad (10)$$

thereby adding another reflectivity parameter  $\gamma$  to our QBH model. The ECO's boundary condition derived from its tidal response is recovered by setting  $\gamma = 4$  [43]. The coefficient  $Y_{\ell m \omega}^{\text{in QBH}}$  can be extracted from  $Y_{\ell m \omega}^{\text{in}}$  by isolating contributions associated with the ringdown phase of the waveform. Converting the radial coefficients to strain components and measuring them at  $\mathcal{I}^+$ , one obtains the strain for the asymptotic echo,

$$h^{\text{echo}} = \sum_n \sum_{\ell, m} -2Y_{\ell m}(\theta, \phi) h_{\ell m, n}^{\text{echo}}(u) \quad (11)$$

where the Fourier transform of the modes  $h_{\ell m, n}^{\text{echo}}(u)$  is given by

$$\begin{aligned} h_{\ell m, n}^{\text{echo}}(\omega) &= \frac{1}{\omega^2} \frac{C}{DD_{\ell m \omega}^{\text{in}}} (\mathcal{R}^{\text{QBH}} \mathcal{R}^{\text{BH}})^n \\ &\quad \cdot \mathfrak{F} \{ C_{\ell m}^{\text{in}} \Psi_{0, \ell m}(v) \mathcal{F}(v) \}. \end{aligned} \quad (12)$$

Here, we define  $\mathfrak{F}(\Psi_{0, \ell m}) =: Y_{\ell m \omega}^{\infty}$  and  $\mathfrak{F}(\cdot)$  denotes the Fourier transform. The coefficient  $\mathcal{R}^{\text{BH}}$  denotes the reflectivity of the BH barrier defined as in [51]<sup>3</sup>. For simplicity, one can introduce a transfer function and rewrite the latter expression as

$$h_{\ell m}^{\text{echo}}(\omega) = \frac{1}{\omega^2} \mathcal{K}(\omega) Y_{\ell m \omega}^{\text{in QBH}} \quad (13)$$

with

$$\begin{aligned} \mathcal{K}(\omega) &= \sum_n \frac{C}{DD_{\ell m \omega}^{\text{in}}} (\mathcal{R}^{\text{QBH}} \mathcal{R}^{\text{BH}})^n \\ &= \frac{(-1)^{\ell+m+1} \mathcal{R}^{\text{QBH}}}{1 - \mathcal{R}^{\text{QBH}} \mathcal{R}^{\text{BH}}} \frac{1}{\gamma D_{\ell m \omega}^{\text{out}}}. \end{aligned} \quad (14)$$

An example of the transfer function is depicted in Figure 2. In the latter, we mark the QBH's QNMs, which appear as poles of the transfer function, as well as the characteristic BH frequencies  $\omega_N$ , which appear as zeros.

**Detecting Gravitational Wave echoes.** Given the reflectivity of the BH horizon and its potential barrier, the echo in equation (12) is fully determined by the waveform at future infinity, as well as the mass and spin of the final BH. With access to the complete asymptotic information including the merger remnant's properties such as redshift, mass, and spin, a detector's ability to measure the echo given by equation (12) can be estimated. In this analysis, we choose LISA to be the relevant detector. To achieve this, we employ the simulation and data analysis pipeline described in [57] and numerically determine the Signal-to-Noise Ratio (SNR) of the echo for a set of 11 numerical relativity simulations. These include *SXS:BBH:1936, 0207, 0334, 1155, 1424, 1448, 1449, 1455, 1936* and *2108*. These events were selected primarily based on their vanishing final spin. Exceptions include *SXS:BBH:0334, 1155, and 2108*, which have remnant spin amplitudes  $|\chi|$  between 0.28 and 0.68. The latter simulations are included in the analysis to check for systematic differences when  $a \neq 0$ . Generally, as the echo computation requires the knowledge of the asymptotic Newman-Penrose scalar  $\Psi_0^{\circ}$  only, any binary merger for which  $\Psi_0^{\circ}$  is available can be used for the SNR computation. However, the extraction of the

<sup>3</sup>Note that in [51],  $\mathcal{R}^{\text{BH}}$  contains a factor of  $1/\gamma = 1/4$  that is attributed to the boundary condition of the ECO considered therein. Changing the boundary condition hence changes  $\mathcal{R}^{\text{BH}}$  as well.

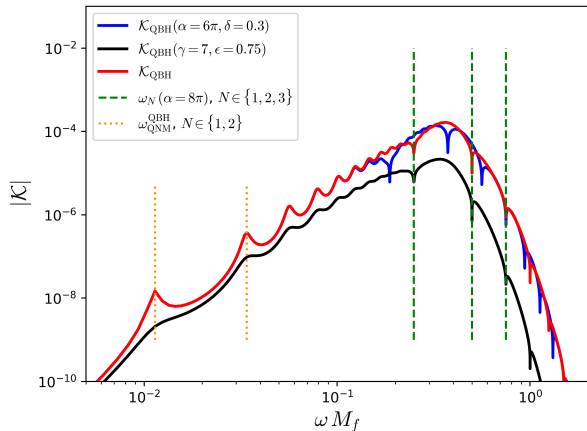


FIG. 2. Transfer function for the standard reflectivity parameter  $\alpha = 8\pi$ ,  $\beta = 10^{-15}$ ,  $\gamma = 4$ ,  $\delta = 0.2$ ,  $\epsilon = 1$ . Any variations in these parameters are indicated.

Newmann-Penrose scalars beyond  $\Psi_4^\circ$  usually requires additional simulation efforts. For *SXS* events, the Cauchy-Characteristic-Evolution (CCE) scheme provides the necessary tools. In particular, we use the CCE method [58, 59] implemented in the new numerical relativity code SpECTRE [60, 61].

A realistic prognosis for detecting GW echoes requires incorporating the sky orientation and position of the sourcing merger event relative to the LISA frame. Regarding the sky position and other orientation-dependent features relevant to the SNR, we adapt the conservative baseline as in Table I of [57]. For reference, the SNR of the full waveform of event *SXS:BBH:1936* is displayed in Figure 3 as a function of redshift and redshifted mass. Compared to the conservative baseline of [57], the SNR in Figure 3 is smaller roughly by a factor of 2. This reduction is primarily due to the different spin components and mass ratios used in their simulations. Note that throughout this work, we compute the echo only for  $h_{2,\pm 2}$ , as the remaining harmonic strain modes are subdominant.

Computing the SNR of the waveform echo, the relevant reflectivity parameters in  $\mathcal{R}^{\text{BH}}$  and  $\mathcal{R}^{\text{QBH}}$  have to be fixed. The choice of these parameters directly impacts the shape of the transfer function  $\mathcal{K}(\omega)$  given by equation (14) (see Figure 2) and therefore the shape of the echo, as demonstrated in Figure 4. We emphasize at this point that not all variables determining the reflectivity in equation (6) yield a significant alteration of the numerically determined SNR value. While the phenomenological constant  $\alpha$  and the cusp-parameter  $\delta$  only influence the location and depth of the roots in Figure 2, the temperature coefficient  $T_{QH}$  (or rather  $\epsilon$ ) and the boundary parameter  $\gamma$  directly impact the amplitude of the transfer function and therefore the amplitude of the echo (compare Figure 4). The time dilation parameter  $\beta$  is irrelevant for the SNR as it only shifts the echo along the time axis, that is, it regulates the time separation be-

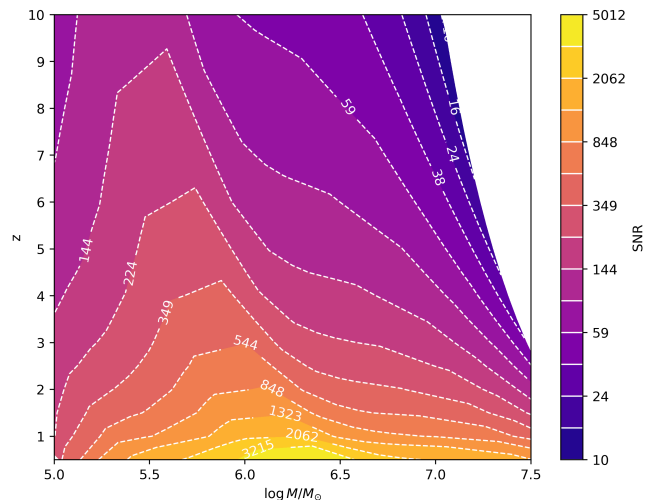


FIG. 3. LISA-SNR of the *SXS:BBH:1936* waveform for different redshifts and total (redshifted) masses. The SNR is computed following [57].

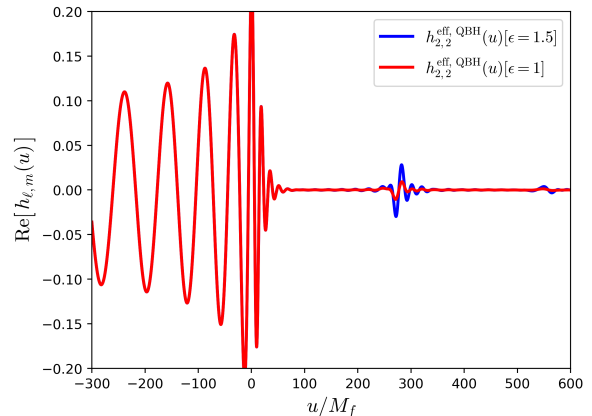


FIG. 4. Exemplary waveform with echo computed for *SXS:BBH:1936* with the standard reflectivity parameter  $\alpha = 8\pi$ ,  $\beta = 10^{-15}$ ,  $\gamma = 4$ ,  $\delta = 0.2$ . The exponential suppression parameter  $\epsilon$  is chosen as indicated.

tween the echo and waveform time series. Generally, we assume that  $\beta$  is small enough such that the echo does not interfere with the ringdown.

Given the different levels of impact that the reflectivity parameter have on the computation of the echo SNR, we first compute the latter using the standard set of variables. That is, choosing  $\alpha = 8\pi$ ,  $\beta = 10^{-15}$ ,  $\gamma = 4$ ,  $\delta = 0.2$ ,  $\epsilon = 1$ , we arrive at the echo displayed in Figure 4 and an echo SNR depending on mass and redshift as in Figure 5<sup>4</sup>. If we fix mass and redshift ( $M_\odot = 10^6$  and  $z = 1$ ), but vary the  $\gamma$  and  $\epsilon$ , the echo SNR is given in

<sup>4</sup>The latter and all following results are displayed only for *SXS:BBH:1936*. We comment on structural differences between events below.

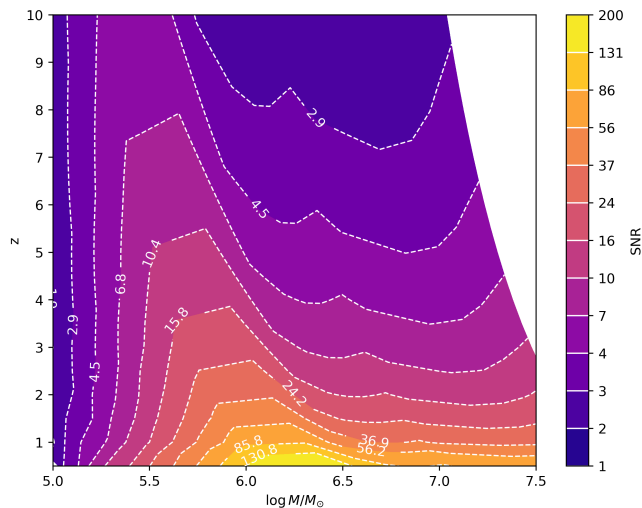


FIG. 5. LISA-SNR of the echo produced by the *SXS:BBH:1936* waveform, depicted in Figure 4, for different redshifts and total (red-shifted) masses. The parameter of reflectivity are chosen as in Figure 4.

6. We normalize the SNR with respect to the standard set of reflectivity parameters ( $\gamma = 4, \epsilon = 1$ ). The normalization enables the simultaneous change of parameters in the SNR: For a given merger determined by redshift and mass, the parameter-dependent echo SNR is given by the product of the SNR value in 5 and the corresponding factor in 6, depending on the choice of reflectivity. For instance, for a merger at redshifted mass  $\log M/M_\odot = 6$  and redshift  $z = 1$ , the SNR for  $\epsilon = 1$  and  $\gamma = 6$  is given by  $\text{SNR} \approx 86 \cdot 0.6 \approx 52$ , where the first value was read of Figure 5, the second of 6. Figure 6 undermines the intuition gained from the transfer function in Figure 2 by demonstrating that, naturally, the SNR decreases for stronger exponential damping in  $\mathcal{R}^{\text{QBH}}$  (smaller  $\epsilon$ ) and weaker reflectivity of the BH horizon (larger  $\gamma$ ). Generally, the results displayed in Figures 5 and 6 clearly demonstrate that, even for very weak echoes that are strongly damped either by the boundary condition or the exponential decay of the reflectivity, the echo SNR in conservative baselines for LISA is large enough ( $\gtrsim 10$ ) such that these echoes could be detected. We emphasize again that, hereby, the time delay plays only a secondary role. Even if the reflection surface is located very close to the horizon, resulting in a large time delay between the initial waveform and the first echo, LISA is able to detect the isolated echo. In this sense, the detectability of echoes is detached from their proximity to the initial merger waveform in the time series. Note, however, that the SNR itself is only an indicator for a detection prospect and relevant detection statistics have to be computed in future work. Further, for the extraction of valuable physical information from echoes the proximity to its sourcing waveform is beneficial as connections to the ringdown can be drawn and the identification of the signal as an echo is more significant. Therefore, we

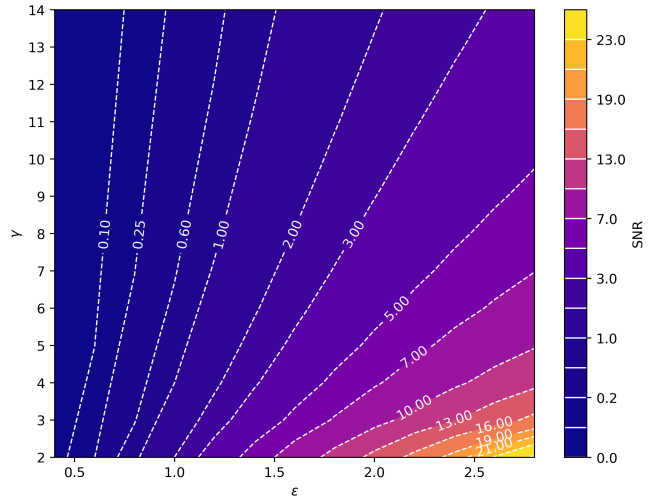


FIG. 6. Normalized SNR for the echo of *SXS:BBH:1936*. We fix  $\log M_\odot = 10^6, z = 1, \alpha = 8\pi, \delta = 0.2$  and vary  $\epsilon, \gamma$ . The resulting SNR is normalized to the SNR resulting from the choice  $\epsilon = 1, \gamma = 4$ , which is  $\approx 13$ .

emphasize that while the time delay of the echo is less relevant for the pure SNR, an actual detection may benefit from echoes residing closer to the ringdown of the BBH merger waveform. For a realistic estimate of the number of potential echo detections, i.e., the number of mergers within a mass and redshift range yielding sufficient SNR, we refer to the discussion in [57]. The latter includes contours for the incidence of events in a certain redshift and mass range that can be transferred one-to-one to this investigation. After testing all listed events, we find that the amplitude of the echoes relative to the merger varies significantly across different events. This variation aligns with expectations, as the amplitude and exact shape of the echoes are primarily influenced by the QNMs of the remnant, which are sensitive to simulation-specific parameters such as the binary mass ratio, spin, and other factors. Among the echoes computed in this study, the simulation *SXS:BBH:1936* represents a relatively conservative choice of a binary merger event in terms of its echo amplitude.

**Measuring Characteristic Frequencies - a Smoking Gun for Black Hole Physics.** Assuming the detection of an echo with LISA, crucial information can be extracted from its features in the interferometer data. Beyond the broader implications regarding the quantum nature of BHs, there is one specific model parameter in the signal's Fourier space data that stands out and can be inferred from the data collected in the Time Delay Interferometry (TDI) channels: the characteristic frequency  $\omega_N$  (in particular its first instance  $\omega_1$ ). As shown in Figure 2, the characteristic frequencies correspond to the roots of the transfer function, which manifest as cusps in the TDI data, as displayed in Figure 7. Detecting characteristic frequencies constitutes a

smoking gun for BH physics as it was pioneered by Beckenstein, Mukhanov, Hawking, and many more. Its measurement would provide a direct probe of the BH entropy formula and the area quantization of the BHs event horizon. Naturally, identifying these roots is constrained by the frequency resolution of the chosen detector, the position of the root within the frequency band, as well as the distinctiveness of the corresponding feature in the data. In the following, we pave the way for in-depth investigations of the detectability of the characteristic frequency by providing a first estimate using the previously LISA data analysis pipeline.

To obtain a first test of the detectability of the characteristic frequency (determined by the fundamental constant  $\alpha$ ) with LISA, given sufficient echo SNR ( $\gtrsim 10$ ), we compute the uncertainty of the associated feature within the TDI X signal<sup>5</sup>. Concretely, we fit the transfer function, Figure 2, to the simulated TDI X data in frequency space, Figure 7, using a non-linear weighted least-squares and a Markov-Chain-Monte-Carlo (MCMC) scheme. The TDI data includes simulated LISA noise following a conservative noise model. The same model has been used in [57]. The fit function is informed about the noise's statistics via its Power Spectral Density (PSD). Figure 7 displays an instance of noisy data (including the TDI X features of an echo) and the pure echo signal without the corresponding merger waveform. The fit is performed with respect to  $\omega_1$ , which can easily be converted to  $\alpha$  using equation (2), and  $\delta$ . The remaining reflectivity parameters are irrelevant to the fitting procedure as they do not modulate the signal amplitude compared to the noise amplitude. An exception is given by  $\epsilon$  as illustrated in Figure 4. For our analysis, we chose  $\epsilon = 1$  as it represents the phenomenologically favored value given the motivation for an exponential decay of the reflectivity, elaborated in detail above. Note that larger  $\epsilon$  generally lead to smaller uncertainties for the identification of  $\omega_1$ , as the signal amplitudes grows in  $\epsilon$ . The uncertainty provided by the fitting schemes is denoted as  $\sigma_{\text{fit}}$ . It represents the the standard deviation error of the fit parameter  $\omega_1$ .

Figure 8 displays the resulting values. Generally, we find that for the colored region, the echo's signal amplitude in the TDI X channel is large enough to yield a fitted characteristic frequency within  $5\sigma$  of the true value and inconsistent with zero. For the uncolored regions, we find that the true value of  $\omega_1$  cannot be meaningfully resolved. For better readability, we truncate Figure 8 at  $\alpha \lesssim 10.22$ . For the tested regime (that is, for  $\log M_{\odot} = 10^6$  and the chosen values of  $\alpha$ ), the characteristic frequencies lay between 1 and 4 mHz. Given a TDI frequency resolution of roughly  $2.5 \mu\text{Hz}$ , even a for  $\sigma_{\text{fit}}/\Delta_{\text{TDI}} \approx 50$  the uncertainty is small enough to obtain a reliable result for

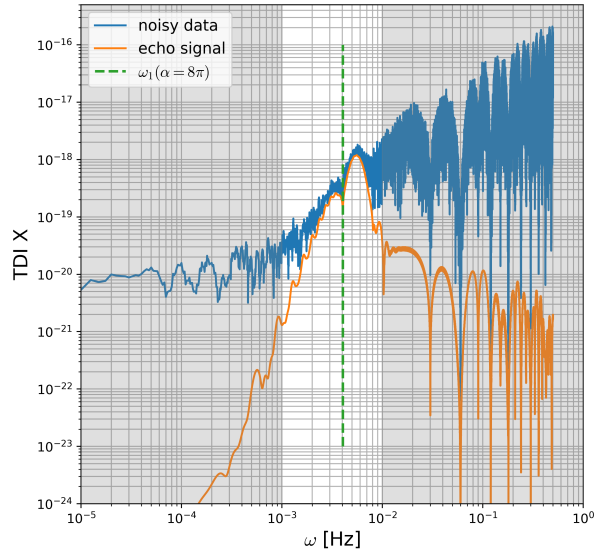


FIG. 7. LISA TDI X channel data for the echo of *SXS:BBH:1936* (including noise) with the standard set of parameter for the reflectivity and  $\delta = 0.5$  at redshift  $z = 1$  and  $\log M_{\odot} = 6$ , including noise. The orange graph represents the signal without noise. The dashed line indicates the location of the first characteristic frequency of the QBH for the given mass and  $\alpha$ . The gray shaded frequency domains are excluded from the fitting procedure.

the characteristic frequencies' locations. As displayed in Figure 8, there is a large region in parameter space for which the first estimate of detectability provided here indicates the possibility of a precise determination of the characteristic frequency value under realistic noise conditions and data analysis techniques. In particular for large  $\alpha$ 's, or equivalently  $\omega_1 \approx 4$  mHz, the uncertainties are small throughout the tested values of  $\delta$ . That is, even for small cusps in the transfer function, the characteristic frequency could be identified if  $\alpha$  is large enough. The results hold true for all tested waveforms listed above.

The displayed trend for the domain of unreliable uncertainties in Figure 8 can be explained by considering the  $\alpha$ -dependent shift of the characteristic frequencies in the TDI data. For lower  $\alpha$ ,  $\omega_1$  and the corresponding cusp move towards the upper end of the noise-dominated low-frequency regime at 1 mHz, see Figure 7. For the chosen approach to identify  $\omega_N$  sufficiently precise when  $\omega_1$  is close to this domain, the cusp-like feature must be pronounced enough, i.e.,  $\delta$  must be larger. Thus, lower  $\alpha$  must be compensated with larger  $\delta$  for reasonably small uncertainty levels. Beyond 1 mHz, the feature of  $\omega_1$  tends to vanish within the noise. The presence of higher order features associated to  $\omega_1$  as the algorithms tend to mistakenly identify, for instance,  $\omega_2$  with  $\omega_1$ . Thus, without the installation of more rigorous priors, uncertain-

<sup>5</sup>There is no particular preference of the X channel. Alternatively, other channels with sufficient signal SNR as well as the full strain data would be eligible for this estimation as well.

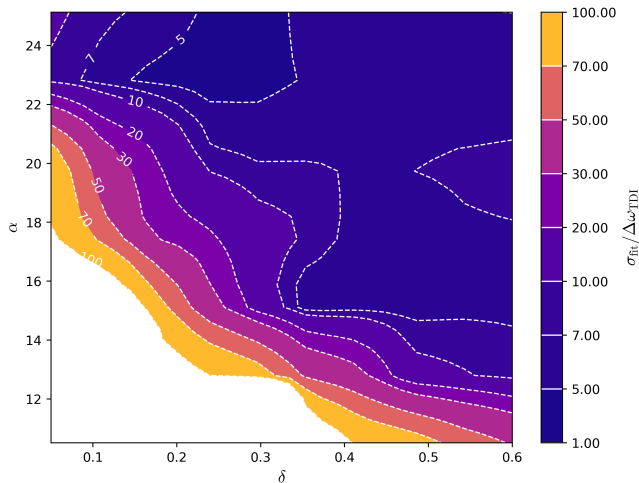


FIG. 8. Uncertainty of the characteristic frequency normalized by the TDI frequency resolution ( $\approx 2.5 \mu\text{Hz}$ ) and extracted from a fit to the TDI data of echo of the simulated waveform *SXS:BBH:1936*. We fix  $\log M_{\odot} = 10^6$ ,  $z = 1$ ,  $\epsilon = 1$ ,  $\gamma = 4$  and vary  $\alpha, \delta$ .

ties in the fitting procedure grow significantly when  $\omega_1$  approaches 1 mHz<sup>6</sup>. We further find that uncertainties reduce as the frequency resolution of the corresponding TDI channel,  $\Delta\omega_{\text{TDI}}$ , decreases. Once  $\Delta\omega_{\text{TDI}}$  reduces below the  $\sigma_{\text{fit}}$  values displayed in Figure 8, the resolution's effects marginalize. This generally matches our expectation as the feature of  $\omega_1$  is narrow in frequency space.

To stress the robustness of this initial analysis, we have performed the analysis over 20 different realizations of the noise. We find that, empirically, the scattering of the 20 recovered frequencies  $\omega_1$  are statistically consistent with the theoretical errors  $\sigma_{\text{fit}}$ . To provide reliable estimates for the detectability, we compute the uncertainty  $\sigma_{\text{fit}}$  via a weighted least squares method and a deeper bayesian MCMC analysis. Thereby, both MCMC and fitting scheme are executed without prior knowledge about the characteristic frequencies location. The MCMC is initiated based on a no-cusp-scenario, i.e.,  $\alpha = 0 = \delta$ . The bounds for  $\alpha$  and  $\delta$  for both methods are set to extend over  $\alpha \in [4 \log 2, 8\pi]$  and  $\delta \in (0.05, 0.5]$ . The tested parameter range of  $\alpha$  is chosen to include all phenomenological constants appearing in literature. For  $\delta$ , we chose a sufficiently large region covering a wide spread of phenomenologies. The uncertainties obtained from the MCMC are consistent with an expected likelihood approach in which the likelihood function of the MCMC is weighted by the noise PSD but the noise realization within the data converges to zero.

Finally, note that when determining the location of the characteristic frequency within LISA's sensitivity band, the remnant's mass can have considerable impact on the uncertainty. Increasing (Decreasing) the mass shifts the characteristic frequency to the lower (higher) frequencies as  $\omega_N \sim 1/M$ . For roughly  $\log M_{\odot} \gtrsim 7.5$  ( $\log M_{\odot} \lesssim 5.5$ ), it exits the sensitivity band of LISA. Thus, coincidentally, the mass domain for which echos are strong and for which the characteristic frequency can potentially be identified, align.

**Discussion.** We developed a phenomenologically motivated toy model for BH reflectivity, based on the assumption that BH area quantization results in a discrete energy spectrum. With non-trivial reflectivity, the BH's QNMs decay in such a way that the ingoing part of the gravitational radiation becomes trapped in a cavity formed between the BH's potential barrier and a reflective shell near the event horizon. Since neither boundary of the cavity is perfectly reflective, this model predicts radiation leakage, manifesting as a GW echo observable by a distant observer.

In this work, we demonstrated that, even under a conservative baseline and moderate echo amplitude, LISA is capable of detecting these gravitational wave echoes originating from the developed QBH model. Notably, the selected range of reflectivity parameters also encompasses values commonly used to describe ECOs, allowing the framework to be applied to both scenarios. Consequently, a non-detection of the echo would significantly constrain both BH and ECO phenomenologies. The forecast regarding the echo's detectability is independent of the exact QNM content and has been analyzed across 11 numerical relativity simulations. For the tested mergers with non-negligible remnant spin, we did not observe any indications of relevant modifications regarding the echo when compared the spin-less remnants. A thorough investigation of the echo construction for spinning BHs and a deeper exploration of connection between QNM content and echo detectability is left to future work. Beyond the echo detection, we showed that across a wide range of masses, redshifts and binary BH mergers, the features in the TDI data corresponding to characteristic frequencies are likely to be detectable to high precision, establishing promising detection prospects. Such a measurement of the characteristic absorption frequency of BHs would provide a direct test of the BH entropy formula and offer stringent constraints on quantum gravity theories. Generally speaking, detecting echo signals provides crucial insights into BH physics and potentially offer direct evidence for quantum gravity effects. Therefore, it is imperative that future space- and ground-based instruments incorporate the search for GW echoes into their scientific agenda.

We acknowledge that several key assumptions in this work - particularly the discrete absorption lines of a physical BH, the reflection of the remaining frequency modes (and the existence of a reflective shell near the horizon), the validity of the boundary condition (10), and the ex-

<sup>6</sup>Note that the concrete frequency regime for which noise dominates changes with the mass of the remnant object, its redshift, the strength of the echo, as well as the instrument under consideration.



ponential decay of  $\mathcal{R}^{\text{QBH}}$  - are either currently debated or are phenomenologically motivated. However, for the purposes of this investigation, these assumptions are sufficient, as our goal is not to establish a fully valid theoretical model but rather to provide a robust proof of concept demonstrating LISA's capability to detect GW echoes. A more rigorous derivation of the mechanisms behind  $\mathcal{R}^{\text{QBH}}$  and  $\mathcal{R}^{\text{BH}}$ , including for instance quantum information theoretical considerations, is left for future work.

Finally, although our analysis has proven robust against substantial variations in certain model parameters, we address the issue of model-dependent echoes within the full GW waveform in a companion paper [62]. There, we delve into the implications of the echo on gravitational wave memory, demonstrating that the resulting signatures are largely model-independent and are directly connected to the energy balance of gravitational radiation being semi-trapped within the cavity.

### ACKNOWLEDGEMENTS

The authors wish to thank Doğa Veske for productive discussion and thank the LISA Simulation Working Group and the LISA Simulation Expert Group for the lively discussions on all simulation-related activities. LH would like to acknowledge financial support from the European Research Council (ERC) under the European Unions Horizon 2020 research and innovation programme grant agreement No 801781. LH further acknowledges support from the Deutsche Forschungsgemeinschaft (DFG, German Research Foundation) under Germany's Excellence Strategy EXC 2181/1 - 390900948 (the Heidelberg STRUCTURES Excellence Cluster). The authors thank the Heidelberg STRUCTURES Excellence Cluster for financial support and acknowledge support by the state of Baden-Württemberg, Germany, through bwHPC. Research at Perimeter Institute is supported in part by the Government of Canada through the Department of Innovation, Science and Economic Development and by the Province of Ontario through the Ministry of Colleges and Universities. This material is based upon work supported by the National Science Foundation under Grants No. PHY-2407742, No. PHY- 2207342, and No. OAC-2209655 at Cornell. Any opinions, findings, and conclusions or recommendations expressed in this material are those of the author(s) and do not necessarily reflect the views of the National Science Foundation. This work was supported by the Sherman Fairchild Foundation at Cornell. This work was supported in part by the Sherman Fairchild Foundation and by NSF Grants No. PHY-2309211, No. PHY-2309231, and No. OAC-2209656 at Caltech.

- 
- [1] S. W. Hawking. Particle Creation by Black Holes. *Commun. Math. Phys.*, 43:199–220, 1975. [Erratum: *Commun. Math. Phys.* 46, 206 (1976)].
- [2] T. Damour. Surface effects in black-hole physics. In *Marcel Grossmann Meeting: General Relativity*, page 587, January 1982.
- [3] Kip S. Thorne, Richard H. Price, and Douglas A. MacDonald. *Black holes: The membrane paradigm*. 1986.
- [4] Richard H. Price and Kip S. Thorne. Membrane viewpoint on black holes: Properties and evolution of the stretched horizon. *Phys. Rev. D*, 33:915–941, Feb 1986.
- [5] Elisa Maggio, Luca Buoninfante, Anupam Mazumdar, and Paolo Pani. How does a dark compact object ring-down? *Physical Review D*, 102(6), September 2020.
- [6] Sumanta Chakraborty, Elisa Maggio, Anupam Mazumdar, and Paolo Pani. Implications of the quantum nature of the black hole horizon on the gravitational-wave ring-down. *Physical Review D*, 106(2), July 2022.
- [7] C. P. Burgess, Ryan Plestid, and Markus Rummel. Effective field theory of black hole echoes. *Journal of High Energy Physics*, 2018(9), September 2018.
- [8] Naritaka Oshita, Qingwen Wang, and Niayesh Afshordi. On reflectivity of quantum black hole horizons. *Journal of Cosmology and Astroparticle Physics*, 2020(04):016–016, April 2020.
- [9] Ivan Agullo, Vitor Cardoso, Adrian del Rio, Michele Maggiore, and Jorge Pullin. Potential gravitational wave signatures of quantum gravity. *Physical Review Letters*, 126(4), January 2021.
- [10] Vitor Cardoso, Valentino F. Foit, and Matthew Kleban. Gravitational wave echoes from black hole area quantization. *Journal of Cosmology and Astroparticle Physics*, 2019(08):006–006, August 2019.
- [11] Valentino F Foit and Matthew Kleban. Testing quantum black holes with gravitational waves. *Classical and Quantum Gravity*, 36(3):035006, Jan 2019.
- [12] Jun Zhang and Shuang-Yong Zhou. Can the graviton have a large mass near black holes? *Physical Review D*, 97(8), April 2018.
- [13] Ruifeng Dong and Dejan Stojkovic. Gravitational wave echoes from black holes in massive gravity. *Physical Review D*, 103(2), January 2021.
- [14] Ahmed Almheiri, Donald Marolf, Joseph Polchinski, and James Sully. Black holes: complementarity or firewalls? *Journal of High Energy Physics*, 2013(2), February 2013.
- [15] Steven B. Giddings. Hawking radiation, the stefan-boltzmann law, and unitarization. *Physics Letters B*, 754:39–42, March 2016.
- [16] Naritaka Oshita and Niayesh Afshordi. Probing microstructure of black hole spacetimes with gravitational wave echoes. *Physical Review D*, 99(4), February 2019.
- [17] Jahed Abedi, Luis Felipe Longo Micchi, and Niayesh Afshordi. Gw190521: Search for echoes due to stimulated hawking radiation from black holes. *Physical Review D*, 108(4), August 2023.
- [18] Kabir Chakravarti, Rajes Ghosh, and Sudipta Sarkar. Signature of nonuniform area quantization on gravitational waves. *Physical Review D*, 104(8), October 2021.
- [19] Qingwen Wang, Naritaka Oshita, and Niayesh Afshordi. Echoes from quantum black holes. *Physical Review D*, 101(2), January 2020.
- [20] Pawel O. Mazur and Emil Mottola. Gravitational vacuum condensate stars. *Proceedings of the National Academy of Sciences*, 101(26):9545–9550, June 2004.
- [21] Matt Visser and David L Wiltshire. Stable gravastars - an alternative to black holes? *Classical and Quantum Gravity*, 21(4):1135–1151, January 2004.
- [22] Thibault Damour and Sergey N. Solodukhin. Wormholes as black hole foils. *Physical Review D*, 76(2), July 2007.
- [23] S.D. Mathur. The fuzzball proposal for black holes: an elementary review. *Fortschritte der Physik*, 53(7):793–827, June 2005.
- [24] Bob Holdom and Jing Ren. Not quite a black hole. *Physical Review D*, 95(8), April 2017.
- [25] Danny Laghi, Gregorio Carullo, John Veitch, and Walter Del Pozzo. Quantum black hole spectroscopy: probing the quantum nature of the black hole area using LIGO–Virgo ringdown detections. *Class. Quant. Grav.*, 38(9):095005, 2021.
- [26] K. G. Arun, Enis Belgacem, Robert Benkel, et al. New horizons for fundamental physics with lisa. *Living Reviews in Relativity*, 25(1), June 2022.
- [27] Nami Uchikata, Tatsuya Narikawa, Hiroyuki Nakano, et al. Searching for gravitational wave echoes from black hole binary events in the third observing run of LIGO, Virgo, and KAGRA collaborations. *Phys. Rev. D*, 108(10):104040, 2023.
- [28] Kabir Chakravarti, Rajes Ghosh, and Sudipta Sarkar. Formation and stability of area quantized black holes. *Phys. Rev. D*, 109(4):046001, 2024.
- [29] Aaron Zimmerman, Richard N. George, and Yanbei Chen. Rogue echoes from exotic compact objects, 2023.
- [30] Elisa Maggio, Vitor Cardoso, Sam R. Dolan, and Paolo Pani. Ergoregion instability of exotic compact objects: Electromagnetic and gravitational perturbations and the role of absorption. *Physical Review D*, 99(6), March 2019.
- [31] Andrew Coates, Sebastian H VÃ¶lkel, and Kostas D Kokkotas. On black hole area quantization and echoes. *Classical and Quantum Gravity*, 39(4):045007, January 2022.
- [32] Andrea Addazi, Antonino Marciano, and Nicolas Yunes. Gravitational instability of exotic compact objects. *The European Physical Journal C*, 80(1), January 2020.
- [33] Baoyi Chen, Yanbei Chen, Yiqiu Ma, Ka-Lok R. Lo, and Ling Sun. Instability of exotic compact objects and its implications for gravitational-wave echoes, 2019.
- [34] Pau Amaro-Seoane, Heather Audley, Stanislav Babak, et al. Laser Interferometer Space Antenna. *arXiv:1702.00786 [astro-ph]*, February 2017. arXiv: 1702.00786.
- [35] Jacob David Bekenstein. Quantum black holes as atoms. *arXiv: General Relativity and Quantum Cosmology*, 1997.
- [36] Emanuele Berti, Vitor Cardoso, and Andrei O Starinets. Quasinormal modes of black holes and black branes. *Classical and Quantum Gravity*, 26(16):163001, July 2009.
- [37] R. A. Konoplya and Alexander Zhidenko. Quasinormal modes of black holes: From astrophysics to string theory. *Reviews of Modern Physics*, 83(3):793–836, July 2011.
- [38] Giovanni Amelino-Camelia. Testable scenario for relativity with minimum length. *Physics Letters B*, 510(1-

- 4):255–263, June 2001.
- [39] James W. York. Black-hole thermodynamics and the euclidean einstein action. *Phys. Rev. D*, 33:2092–2099, Apr 1986.
- [40] Jacob D. Bekenstein and V.F. Mukhanov. Spectroscopy of the quantum black hole. *Physics Letters B*, 360(1-2):7–12, October 1995.
- [41] Shahar Hod. The quantum emission spectra of rapidly-rotating kerr black holes: Discrete or continuous? *Physics Letters B*, 749:115–118, October 2015.
- [42] Jahed Abedi, Hannah Dykaar, and Niayesh Afshordi. Echoes from the abyss: Tentative evidence for planck-scale structure at black hole horizons. *Phys. Rev. D*, 96:082004, Oct 2017.
- [43] Baoyi Chen, Qingwen Wang, and Yanbei Chen. Tidal response and near-horizon boundary conditions for spinning exotic compact objects. *Phys. Rev. D*, 103:104054, May 2021.
- [44] Samir D. Mathur and David Turton. Comments on black holes i: the possibility of complementarity. *Journal of High Energy Physics*, 2014(1), January 2014.
- [45] Borun D. Chowdhury and Andrea Puhm. Decoherence and the fate of an infalling wave packet: Is alice burning or fuzzing? *Physical Review D*, 88(6), September 2013.
- [46] Avery E. Broderick, Abraham Loeb, and Ramesh Narayan. The event horizon of sagittarius a\*. *The Astrophysical Journal*, 701(2):1357–1366, July 2009.
- [47] Avery E. Broderick, Ramesh Narayan, John Kormendy, et al. The event horizon of m87. *The Astrophysical Journal*, 805(2):179, June 2015.
- [48] Niayesh Afshordi and Yasaman K Yazdi. Firewall phenomenology with astrophysical neutrinos. *Classical and Quantum Gravity*, 33(23):235017, November 2016.
- [49] Ue-Li Pen and Avery E. Broderick. Possible astrophysical observables of quantum gravity effects near black holes. *Monthly Notices of the Royal Astronomical Society*, 445(4):3370–3373, October 2014.
- [50] Qingwen Wang and Niayesh Afshordi. Black hole echology: The observer’s manual. *Phys. Rev. D*, 97:124044, Jun 2018.
- [51] Sizheng Ma, Qingwen Wang, Nils Deppe, et al. Gravitational-wave echoes from numerical-relativity waveforms via spacetime construction near merging compact objects. *Physical Review D*, 105(10), May 2022.
- [52] S. A. Teukolsky and W. H. Press. Perturbations of a rotating black hole. III. Interaction of the hole with gravitational and electromagnetic radiation. *Astrophys. J.*, 193:443–461, October 1974.
- [53] A. A. Starobinsky. Amplification of waves reflected from a rotating "black hole". *Sov. Phys. JETP*, 37(1):28–32, 1973.
- [54] Scott A. Hughes. Evolution of circular, nonequatorial orbits of kerr black holes due to gravitational-wave emission. *Phys. Rev. D*, 61:084004, Mar 2000.
- [55] Shuo Xin, Baoyi Chen, Rico K. L. Lo, et al. Gravitational-wave echoes from spinning exotic compact objects: Numerical waveforms from the teukolsky equation. *Phys. Rev. D*, 104:104005, Nov 2021.
- [56] Black Hole Perturbation Toolkit. (bhptoolkit.org).
- [57] Henri Inchauspe, Silvia Gasparotto, Diego Blas, et al. Measuring gravitational wave memory with lisa, 2024.
- [58] Jordan Moxon, Mark A. Scheel, and Saul A. Teukolsky. Improved cauchy-characteristic evolution system for high-precision numerical relativity waveforms. *Physical Review D*, 102(4), August 2020.
- [59] Jordan Moxon, Mark A. Scheel, Saul A. Teukolsky, et al. The spectre cauchy-characteristic evolution system for rapid, precise waveform extraction, 2021.
- [60] Lawrence E. Kidder, Scott E. Field, Francois Foucart, et al. Spectre: A task-based discontinuous galerkin code for relativistic astrophysics. *Journal of Computational Physics*, 335:84–114, April 2017.
- [61] Nils Deppe, William Throwe, Lawrence E. Kidder, et al. SpECTRE v2024.06.18. 10.5281/zenodo.12098412, 6 2024.
- [62] Nils Deppe, Lavinia Heisenberg, Henri Inchauspe, et al. Potential signatures of quantum gravity in the gravitational wave memory effect, 2024.